ACS APPLIED MATERIALS & INTERFACES

Research Article

www.acsami.org

Detection of Volatile Organic Compounds Using Microfabricated Resonator Array Functionalized with Supramolecular Monolayers

Yao Lu, Ye Chang, Ning Tang, Hemi Qu, Jing Liu, Wei Pang,* Hao Zhang, Daihua Zhang, and Xuexin Duan*

State Key Laboratory of Precision Measuring Technology & Instruments, College of Precision Instrument and Opto-Electronics Engineering, Tianjin University, Tianjin 300072, China

Supporting Information

ABSTRACT: This paper describes the detection of volatile organic compounds (VOCs) using an e-nose type integrated microfabricated sensor array, in which each resonator is coated with different supramolecular monolayers: *p-tert*-butyl calix[8]-arene (Calix[8]arene), 2,3,7,8,12,13,17,18-octaethyl-21H,23H-porphine (Porphyrin), β-cyclodextrin (β-CD), and cucurbit[8]uril (CB[8]). Supramolecular monolayers fabricated by Langmuir–Blodgett techniques work as specific sensing interface for different VOCs recognition which increase the sensor selectivity. Microfabricated ultrahigh working frequency film bulk acoustic resonator (FBAR) transducers (4.4 GHz) enable their high sensitivity toward monolayer gas sensing which facilitate the analyses of VOCs adsorption isotherms and kinetics. Two affinity constants (K_1, K_2) are obtained for each VOC, which indicate the gas molecule adsorption happen inside and outside of the supramolecular cavities. Additional kinetic information on adsorption and desorption rate constants (k_a, k_d) are obtained as well from exponential fitting results. The five parameters, one from the conventional frequency shift signals of mass transducers and the other four from the indirect analyses of monolayer adsorption behaviors, thus enrich the sensing matrix (Δf, K_1, K_2, k_a, k_d) which can be used as multiparameter fingerprint patterns for highly selective detection and discrimination of VOCs.

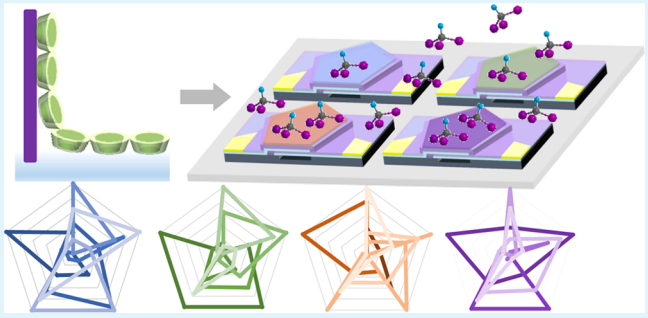

KEYWORDS: *resonator array, electronic nose, supramolecular chemistry, Langmuir–Blodgett films, VOCs, adsorption isotherms, kinetics*

1. INTRODUCTION

Over the past decade, development of portable gas sensors that can be used for on-site and real-time detection of volatile organic compounds (VOCs) has been of great significance in the fields of environmental monitoring, chemical warfare, explosive detection, and health assessment.[1−4] VOCs are participants in the reaction of atmospheric photochemistry and can be used as biomarkers contained in the exhaled breath from cancer patients for diagnoses purposes and for monitoring the treatments of the diseases.[5−8] Although some portable gas sensors are commercially available, such as sensing devices integrated with photoionization detector, they cannot distinguish between different VOCs and the cross reactivity in complex vapor mixtures remains a major challenge in this concise way.[9]

So far, electronic nose (e-nose) sensor array which comprises a large number of different sensors coupled with pattern-recognition protocols is one of the most successful platforms for VOCs discriminations.[10] In each sensor of e-nose system, chemically sensitive layer for target gas molecule detection is coupled with a transducer which transforms the interactions between the gas molecules and chemical coatings into readable signals. In most electronic noses, each sensor is sensitive to all volatile molecules but each in their specific way; thus, a fingerprint pattern is generated for specific target recognition. Acoustic wave (AW) transducers, such as quartz crystal microbalance (QCM)[11−14] and surface acoustic wave (SAW) resonators[15−18] are popular sensor components for an e-nose set. They generate acoustic waves and measure the variation of the wave propagation properties as a signal of frequency shift for probing the mass uptake of a sensing layer when exposed to vapors.[19] Surface functionalization of the sensors plays a key role in molecule recognitions, and it directly controls the sensor sensitivity, selectivity, stability, and reversibility.[20,21] Polymer coatings are the most popular surface functionalization of e-noses; however, such modification process is complex and the selectivity is too low to distinguish between different kinds of VOCs.[22,23] Besides, it suffers the irreversible gas adsorption into thick polymer layers which may induce the malfunctions of the e-noses.[24,25] Achieving effective molecular recognition at the gas–solid interface is a demanding task for e-nose applications. In recent years, supramolecular coatings have been applied in

Received: May 20, 2015
Accepted: July 30, 2015
Published: July 30, 2015

DOI: 10.1021/acsami.5b04385
ACS Appl. Mater. Interfaces 2015, 7, 17893−17903

Scheme 1. (a) Schematic of a FBAR Sensor Array Functionalized with Four Supramolecular Monolayers, (b) Sectional View of the FBAR Structure, and (c) Top View of Scanning Electron Micrograph (SEM) Image of a FBAR

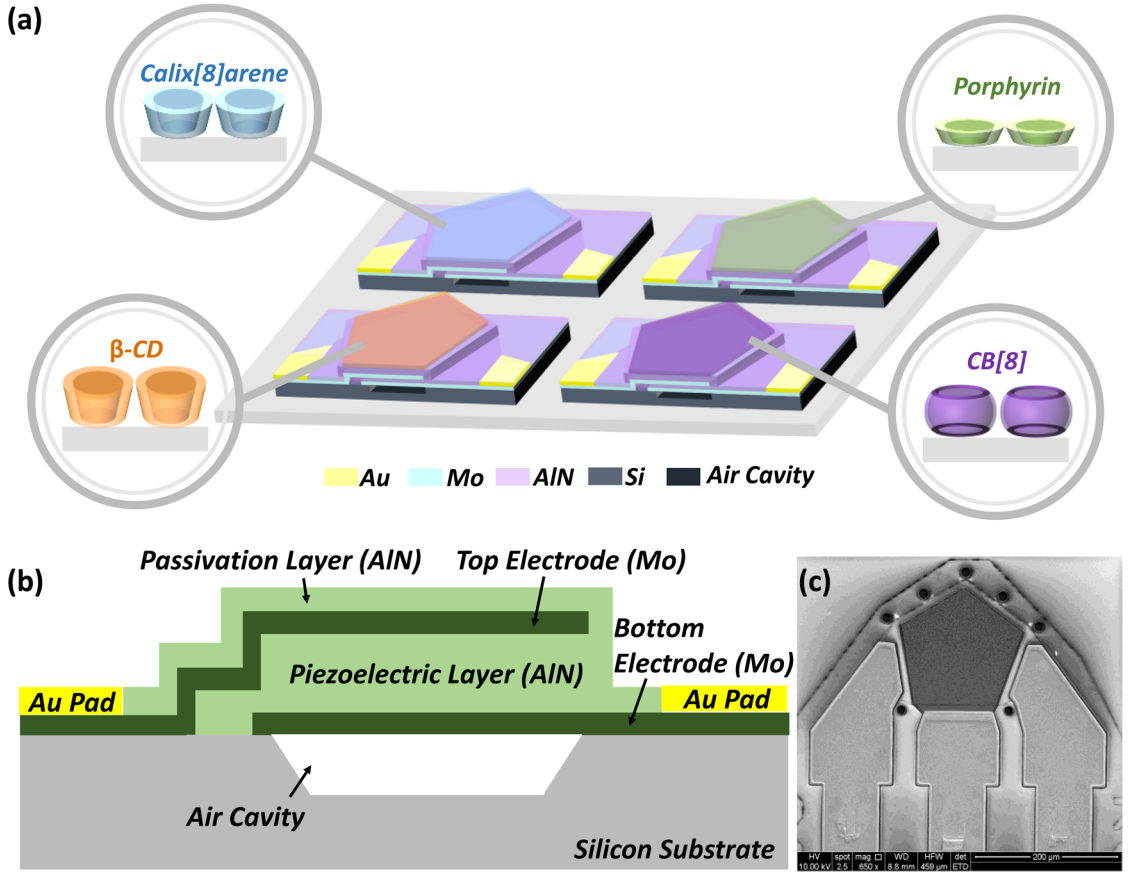

the detection of VOCs. Because of their specific "host−guest" interactions, supramolecular coatings increase the sensor specificity and accuracy.[26−29] For instance, multiple layers of porphyrin and its derivatives have been deposited on QCM to detect *n*-propyl alcohol (NPA), chloroform, and toluene;[30−32] Calix[*n*]arenes have been used as well for VOCs detections.[33−35] However, most of the previous studies are using multiple layers of supramolecules which suffer less specificity and low reversibility due to the gas molecule nonspecific adsorption between the multilayers of supramolecules. Besides, the gas molecule adsorption isotherms and kinetics are less covered in these studies, since it normally requires longer contact time to get stable sensor signals which is partially due to the target molecule noncontrollable diffusion into the receptor multiple layers. The operating frequency range of QCM or SAW device is only several MHz to dozens of MHz, which decides a restricted sensitivity and sets a limit to the utilization of multiple layers of supramolecules in order to adsorb more VOCs to enhance frequency response.

In this work, we fabricated film bulk acoustic resonators (FBARs) with ultrahigh working frequency (4.4 GHz) as mass transducers to evaluate different monolayers of supramolecular coatings for their gas recognition behaviors. FBAR sensors have been demonstrated as promising biosensor for detections of DNA hybridizations,[36] protein adsorptions,[37] and other biomolecule interactions.[19] The applications of such types of sensors as selective gas sensors are less covered.[38] Since they have important features of miniature device sizes, high quality factor (*Q*), and compatibility with complementary metal oxide semiconductor (CMOS) technology,[39] FBARs are beneficial to be integrated as sensor arrays for e-nose applications. Here, an array of FBAR gas sensors was created with the coatings of four different amphiphilic supramolecular monolayers through Langmuir−Blodgett (LB) process (*p-tert*-butyl calix[8]arene (Calix[8]arene), 2,3,7,8,12,13,17,18-octaethyl-21*H*,23*H*-porphine (Porphyrin), *β*-cyclodextrin (*β*-CD), and cucurbit[8]uril (CB[8])). Benefit from the monolayer coatings, fast and reversible detection of VOCs, was realized by monitoring the supramolecular gas phase "host−guest" interactions with high frequency FBAR sensors vibrating at 4.4 GHz. The functional groups at the interface of monolayer coatings behaved differently amphiphilically and acted as molecular recognition sites for vapor molecules with increased sensor selectivity. The adsorption isotherms of supramolecular monolayers toward different VOCs were fitted using a dual-site Langmuir−Freundlich (DSLF) equation. The adsorption and desorption rate constants of the four functional monolayers with different VOCs have also been obtained with kinetic analyses; thus, these constants can be used as additional sensing parameters to enrich the library of gas recognition fingerprints for selective VOCs detections. The demonstrated FBAR sensor arrays are promising candidates as a new type of e-nose gas sensors, and the studies of the supramolecular coatings would benefit the developing of new interface materials for gas sensor applications.

DOI: 10.1021/acsami.5b04385
ACS Appl. Mater. Interfaces 2015, 7, 17893−17903

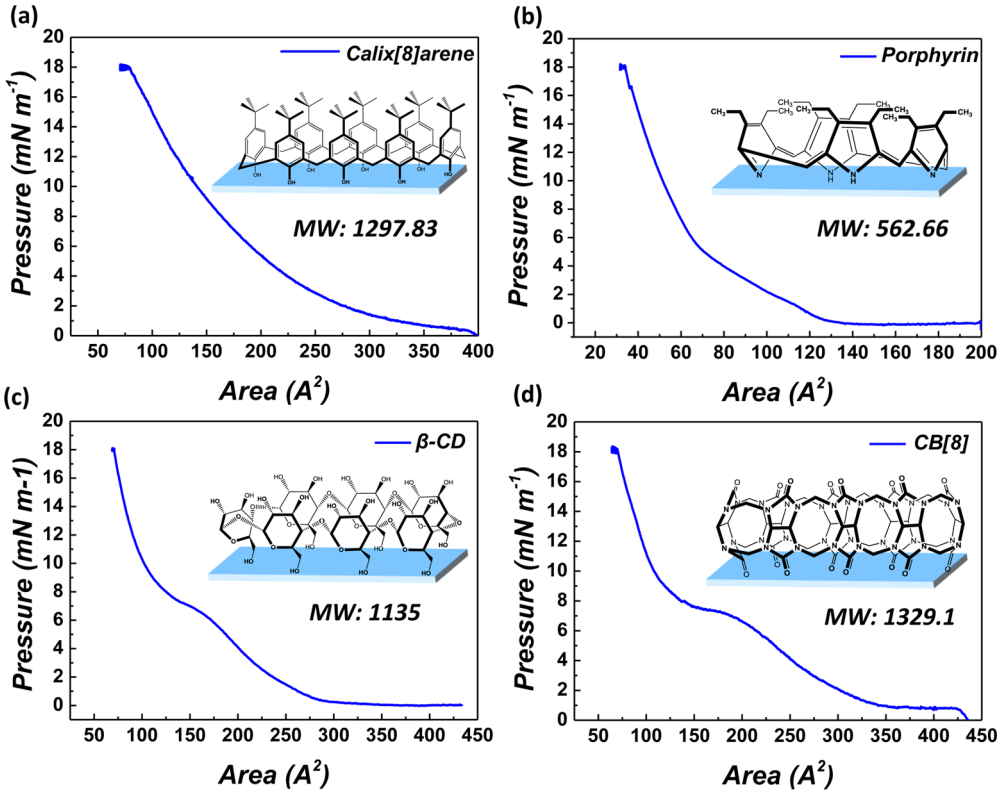

Figure 1. π–A compression isotherms and chemical structures of supramolecular monolayers of (a) Calix[8]arene, (b) Porphyrin, (c) β-CD, and (d) CB[8].

2. EXPERIMENTAL SECTION

2.1. Materials. *p-tert*-Butyl calix[8]arene (Calix[8]arene), 2,3,7,8,12,13,17,18-octaethyl-21H,23H-porphine (Porphyrin), β-cyclodextrin (β-CD), and cucurbit[8]uril (CB[8]) were purchased from Sigma-Aldrich and utilized without further purification. HPLC-grade VOCs (chloroform, acetone, *n*-propyl alcohol (NPA), methanol, hexane, and cyclohexane) were purchased from Tianjin Yuanhua and used as received with no further purification.

2.2. Device Fabrication. In this work, film bulk acoustic resonators (FBARs) were fabricated using standard microfabrication according to a previous published process (see also Supporting Information).[40] The series resonant frequency signal of FBAR was obtained by network analyzer (Agilent E5061B).

2.3. Device Functionalization. The aluminum nitride (AlN) substrates and FBAR sensors were oxidized in air plasma for 5 min to form hydrophilic interface with plasma cleaner. The resulting hydrophilic surfaces were coated with supramolecular monolayers using Langmuir–Blodgett (LB) trough (Kibron Micro-Trough XS). All compounds were dissolved in chloroform with a typical concentration of 0.2 mg mL^{-1} and filtered by 0.22 μm Teflon membranes. Among the four supramolecular compounds, Calix[8]-arene, β-CD, and CB[8] are less soluble; a short sonication treatment is required to get them fully dissolved in chloroform. An amount of 50 μL of each filtered solutions was spread onto the precleaned water subphase with a pipet and then compressed at the speed of 10 mm min^{-1} until the surface pressure reached 18 mN m^{-1}. Afterward, the substrates (or devices) were pulled up vertically from the subphase interface at a constant speed of 1 mm min^{-1}; thus, regularly arranged supramolecular monolayers were coated on the substrates.

2.4. Surface Characterization. The supramolecular monolayers coating on AlN substrates were characterized by contact angle (CA) measurements (JC2000DM, Zhongchen), Fourier transform infrared (FT-IR) spectrometry (Vertex 70v, Bruker Optics, Germany), and atomic force microscopy (AFM, Veeco, Nano Scope III) in tapping mode.

2.5. VOCs Detection System. Figure S2 shows the VOCs detection setup (see Supporting Information). The system consisted of two gas channels. One channel produced saturated VOC vapors by bubbling nitrogen gas through VOC liquids in a glass bubbler, the flow velocity of which was monitored by a mass flow controller (MFC). The other one carried out pure nitrogen gas and joined in the VOCs channel at a confluence to form a mixed channel, which guided VOC vapors to the sensor surfaces. Nitrogen gas (99.999%) was used as background gas to avoid the influence by the humidity effect. Experiments were conducted with sequent exposure to VOCs at 10 different concentrations in terms of P/P_0 from 0.1 to 1, where P stands for the partial pressure of the VOCs and P_0 stands for the saturated vapor pressure at room temperature.

3. RESULTS AND DISCUSSION

3.1. FBAR Sensor Array. Scheme 1a shows the schematic of a functionalized FBAR sensor array used in this work. The four FBARs were coated with monolayers of Calix[8]arene, Porphyrin, β-CD, and CB[8], respectively, and bonded on a printed circuit board (PCB) to form an integrated sensor array. A typical sandwiched structure of FBAR comprises two molybdenum (Mo) layers as electrodes (top electrode and bottom electrode) and a piezoelectric layer of aluminum nitride (AlN) in the middle to generate acoustic waves (see Scheme 1b). An additional passivation layer of AlN is deposited on the top electrode to prevent oxidation and corrosion and to function as an interface for supramolecular coatings. Scheme 1c presents the top view of scanning electron microscope (SEM) image of a FBAR.

3.2. Compression Isotherms. In this work, we selected four different amphiphilic supramolecular coatings (Calix[8]-arene, Porphyrin, β-CD, and CB[8]). Calix[8]arene and Porphyrin have similar structures that one brim of the molecule

DOI: 10.1021/acsami.5b04385
ACS Appl. Mater. Interfaces 2015, 7, 17893–17903

is hydrophobic (alkyl group) and the other side is hydrophilic (hydroxyl or amino group). β-CD and CB[8] both are class of macrocyclic hosts with a rigid hydrophobic cavity and two identical fringed portals (see chemical structures in Figure 1). The surface pressure−area (π−A) compression isotherms of the four supramolecules are shown in Figure 1.

During the film fabrication process, the same quality of each compound was applied in the LB trough; thus, the occupied space per unit molecule is approximately proportional to the molecular weight (MW) of the molecule. This agreed with the compression isotherms as shown in Figure 1. Porphyrin monolayer shows the smallest area per molecule (200 Å^2). The MW of Calix[8]arene, β-CD, and CB[8] is approximately twice of that of porphyrin; thus, the area per molecule is almost double. Different types of π−A compression isotherms appeared which is due to their different chemical structures and amphiphilic properties. The transition points of molecular phase are clear on the Porphyrin monolayer π−A curve but inconspicuous for Calix[8]arene. The S-type π−A curves of β-CD and CB[8] mean that the macrocyclic host molecules form monolayers under higher surface pressure. All these results indicated that well-organized monolayers of supramolecules were formed on the water subphase.

The monolayers of supramolecules were transferred to the devices at a constant pressure, considering of the film stability at such pressure and better comparison of their gas recognition behaviors. We have compared the LB films formed at different fixed surface pressures (at 12, 15, and 18 mN m^{-1}, respectively) and further tested their VOCs detection. The results showed that with the increasing of the surface pressure during the formation of the LB films, the frequency shifts to the same VOC adsorption increased, which indicated that higher molecular density would result in more VOC adsorptions. However, when the surface pressure continued increasing, the frequency response to VOCs dropped, which was likely due to the collapse of supramolecular monolayers at higher compression pressures. Thus, we found that 18 mN m^{-1} was the most appropriate value for the formation of densely packed supramolecular monolayers for VOC detection.

3.3. Characterization. *3.3.1. Contact Angle Measurements.* Water contact angle (CA) measurements were used to characterize the fabricated supramolecular LB films on flat AlN substrates (see also the Supporting Information, Figure S3). After plasma treatment, AlN substrate becomes superhydrophilic (CA is below 4°). After deposition of amphiphilic monolayers, the CA values of Calix[8]arene and Porphyrin turn into 107° and 82°, indicating that the interfaces are hydrophobic. On the contrary, the AlN substrates coated with β-CD and CB[8] remain hydrophilic with repeatable CA values of 55° and 61°. This result confirms the molecule orientations of the supramolecular monolayers. The relations between the hydrophilicity of the interface and the gas adsorption are in fact the interactions between functional groups of supramolecular monolayers and VOCs molecules; thus, the hydrophobicity and hydrophilicity of the top layers can be used to distinguish different types of gas molecules and applied in the VOCs selective detection.

3.3.2. FT-IR Spectrometer Tests. FT-IR spectra were used to characterize the LB films on AlN surfaces. It was obtained using an IR spectrometer equipped with an attenuated total reflection (ATR) accessory. A liquid nitrogen cooled mercury−cadmium−telluride (MCT) detector was used to record the FT-IR spectra at permanent vacuum condition. With the above characteristics, the monolayers of LB films could be analyzed with high sensitivity. Figure 2 shows the FT-IR reflection spectra of the four supramolecular monolayers coated on AlN substrates.

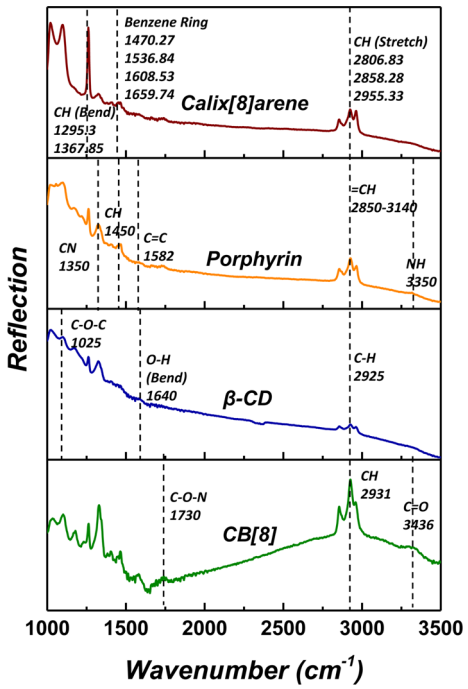

Figure 2. FT-IR reflection spectra of Calix[8]arene, Porphyrin, β-CD, and CB[8].

Calix[8]arene monolayer shows characteristic peaks at 1470 and 1536 cm^{-1} which are assigned to the band of benzene ring. The peaks of C−H stretching frequency appear at 2858 and 2955 cm^{-1}, whereas the peaks of C−H bending frequency appear at 1295 and 1368 cm^{-1}.[41] For Porphyrin monolayer, the N−H stretching frequency is found to be weak at 3350 cm^{-1} which contains hydrogen bonding in the condensed ring systems. The peaks at 2850−3140 cm^{-1} are due to =C−H stretching vibrations. The skeletal in-plane conjugated phenyl C=C vibrates near 1582 cm^{-1}, and the strong frequency near 1350 cm^{-1} is tentatively assigned to the C−N stretching vibration.[42] In the FT-IR spectra of β-CD monolayer, the peaks at about 1028, 1640, and 2925 cm^{-1} can be indexed to C−H, O−H, and C−O−C groups, respectively.[43,44] CB[8] monolayer exhibits characteristic peaks at 1730, 2931, and 3436 cm^{-1} indicative of CO−N, C−H, and C=O stretching, respectively.[45]

Besides FT-IR, we performed energy dispersive spectroscopy (EDS) on the same supramolecular monolayers (see Table S1 in Supporting Information). The element contents of the four supramolecular coatings are consistent with their molecular structures. All these results confirm the successful formation of supramolecular monolayers on AlN substrates.

3.3.3. Surface Morphology Analysis. Furthermore, the surface morphology of the supramolecular LB films is characterized by AFM with a tapping mode (see Figure 3). The shapes of the four supramolecular coatings are rather similar, and the average height is 2.83 ± 0.86 nm, 1.84 ± 0.35 nm, 1.87 ± 0.52 nm, and 4.25 ± 0.97 nm for Calix[8]arene, Porphyrin, β-CD, and CB[8], respectively, which indicates the

DOI: 10.1021/acsami.5b04385
ACS Appl. Mater. Interfaces 2015, 7, 17893−17903

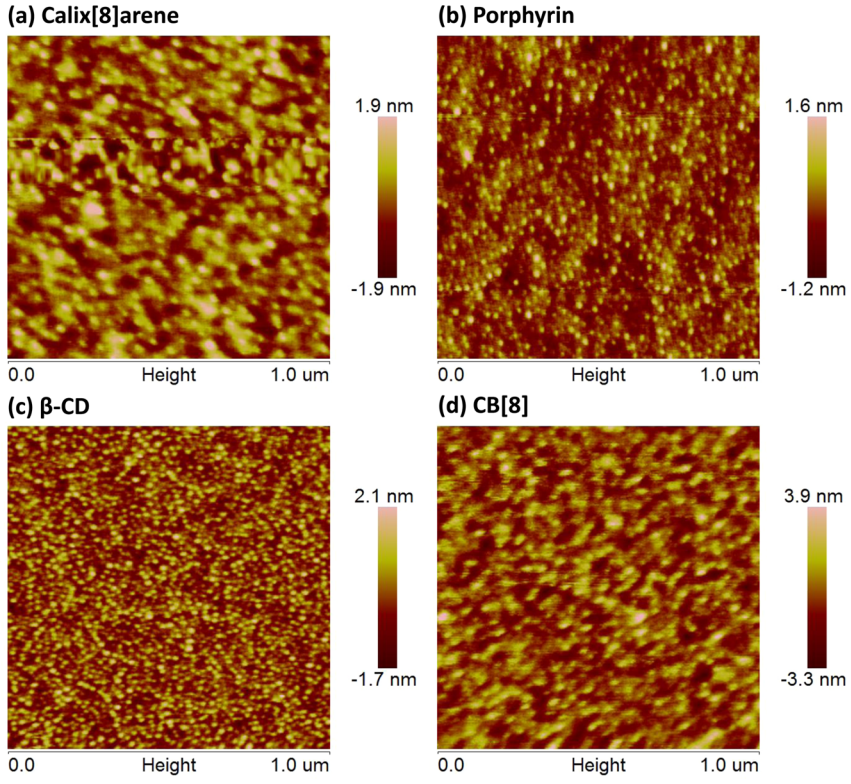

Figure 3. AFM images of the supramolecular coatings of (a) Calix[8]arene, (b) Porphyrin, (c) β-CD, and (d) CB[8].

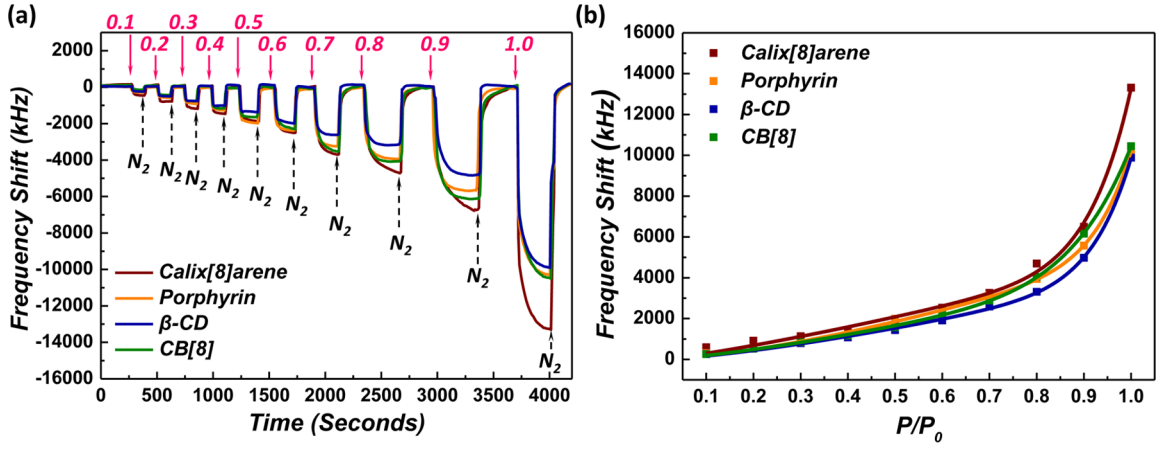

Figure 4. (a) Real-time sensor responses of the FBAR sensor array functionalized with supramolecular monolayers with exposure to chloroform at 10 different concentrations in terms of P/P_0 from 0.1 to 1 (i.e., the red numbers labeled inside (a)), where P stands for the partial pressure of chloroform and P_0 stands for the saturated chloroform pressure at room temperature. (b) Adsorption isotherms of chloroform. The dots represent the measuring data, and the solid lines represent the fitting results with eq 2.

formation of smooth supramolecular monolayers on AlN substrates.

3.4. VOCs Detection Results. As described in Sauerbrey's eq 1,[19] when adding a layer of mass loading on the top of FBAR, the series resonant frequency decreases linearly to the mass loading in accordance. Higher working resonance frequency will induce more frequency shift with the same mass loading on the sensor surface. In this work, we applied ultrahigh resonance frequency FBARs as the transducers (4.4 GHz), which are able to measure the small mass change by the adsorption of VOCs to the monolayers of supramolecular receptors.

$$\frac{\Delta f}{f_0} \approx \frac{\rho_m d_m}{\rho_0 d_0} \quad (1)$$

Here f_0 and Δf are the resonance frequency of FBAR and frequency shift after adsorption of VOCs. ρ_m and ρ_0 are the mass density of adsorption layer and resonator itself, respectively. d_m and d_0 are the thickness of the adsorption layer and resonator.

3.4.1. Real-Time Sensor Responses of the FBAR Sensor Array. Figure 4a shows the real-time sensor responses of the FBAR sensor array functionalized individually with monolayers of Calix[8]arene, Porphyrin, β-CD, and CB[8] in exposure to chloroform vapors at 10 different concentrations.

DOI: 10.1021/acsami.5b04385
ACS Appl. Mater. Interfaces 2015, 7, 17893−17903

Table 1. Adsorption Affinity Constants of Six VOCs Fitted by DSLF Equation

	affinity constant							
	Calix[8]arene		Porphyrin		β-CD		CB[8]	
VOC	$K_1 \times 10^{-2}$	$K_2 \times 10^{-2}$	$K_1 \times 10^{-2}$	$K_2 \times 10^{-2}$	$K_1 \times 10^{-2}$	$K_2 \times 10^{-2}$	$K_1 \times 10^{-2}$	$K_2 \times 10^{-2}$
chloroform	3.0 ± 0.2	0.63 ± 0.04	1.2 ± 0.7	0.93 ± 0.02	2.1 ± 0.2	0.67 ± 0.04	2.7 ± 0.4	1.23 ± 0.05
acetone	3.5 ± 0.4	0.82 ± 0.05	1.7 ± 0.4	0.74 ± 0.03	1.5 ± 0.6	0.71 ± 0.07	1.0 ± 0.5	0.79 ± 0.06
NPA	2.2 ± 0.7	0.91 ± 0.04	1.1 ± 0.8	1.04 ± 0.06	1.1 ± 0.5	0.91 ± 0.04	1.2 ± 0.3	1.01 ± 0.06
methanol	5.2 ± 0.3	0.91 ± 0.02	3.4 ± 0.6	1.25 ± 0.07	1.2 ± 0.7	0.94 ± 0.06	5.1 ± 0.6	0.82 ± 0.07
hexane	2.8 ± 0.5	0.75 ± 0.08	4.8 ± 0.4	1.12 ± 0.06	1.4 ± 0.4	1.01 ± 0.08	2.0 ± 0.7	1.11 ± 0.04
cyclohexane	4.1 ± 0.4	1.01 ± 0.07	1.5 ± 0.5	0.82 ± 0.04	2.4 ± 0.4	0.82 ± 0.03	3.9 ± 0.2	0.87 ± 0.03

Scheme 2. VOCs Adsorption on Supramolecular Monolayers[a]

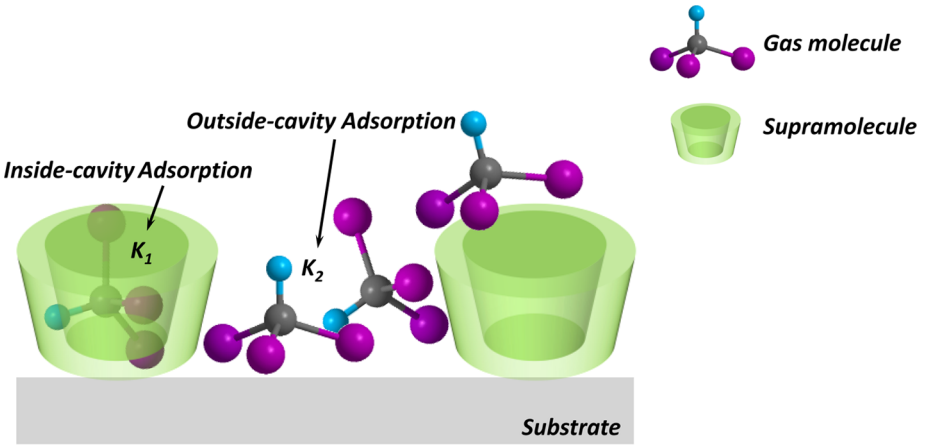

[a]Gas molecules can adsorb inside and outside the cavity of supramolecules.

The FBAR sensor array was first flushed with nitrogen gas to reach a stable baseline, and 10 sensing cycles were performed. A sensing cycle comprised both VOCs absorption and desorption. In the adsorption process, chloroform vapor was introduced to the functionalized FBAR sensors and negative resonance frequency shifts were observed, indicating the quick adsorption of gas molecules to the supramolecular monolayers.

The attachment of the VOCs to the supramolecular monolayers is maintained by the van der Waals forces for the presented device. The van der Waals forces between the VOCs molecules and supramolecular monolayers are weak; thus, the interactions are concentration dependent and reversible. After switching to nitrogen, the concentration of VOCs became zero and the van der Waals forces did not maintain balance; thus, the VOCs molecules were blow off by the nitrogen gas. As shown in Figure 4a, in the desorption process, the resonance frequency went up quickly and returned to the baseline. These results demonstrate the merit of quick response and full recovery of supramolecular monolayers coated FBAR sensors for VOCs detections.

The sensor responses of the FBAR sensor array coated with different supramolecular monolayers behave discriminatively in Figure 4a. The main reason is the different van der Waals force between the gas molecules and the supramolecular receptors. The interface of Calix[8]arene and Porphyrin proved to be hydrophobic in the CA tests, which is suitable for the absorption of hydrophobic chloroform molecules, while the adsorption happening on hydrophilic β-CD and CB[8] is different. It is likely that the chloroform molecules prefer to enter the hydrophobic cavities of these macrocyclic hosts and interact with interior groups. For β-CD, it shows the most hydrophilic property which is not favorable for VOC molecules to enter its cavity so that the frequency shifts are smaller compared to those of the other three compounds in most situations. Beside the hydrophilicity, the sensor response is a comprehensive result of multiple factors. The size of the supramolecular cavity and the species of the functional groups on the interface affect the sensor response as well. Real-time sensor responses of the other five VOCs (acetone, *n*-propyl alcohol (NPA), methanol, hexane, and cyclohexane) were obtained using the same four supramolecules coated FBAR sensor array (see Figure S4, Supporting Information).

3.4.2. Adsorption Isotherms of VOCs on Supramolecular Monolayers. The adsorption isotherms of chloroform on four supramolecular monolayers were plotted in Figure 4b. The adsorption isotherms show a two-step adsorption process. In low concentration range (P/P_0 below 0.8), the adsorbed gas molecules increased slowly with the increased gas concentration, while in the second process, the adsorbed molecules increased much more quickly and when the VOCs concentration is close to their saturated pressure, the frequency shifts of FBAR sensors increase to a higher level rather than terminate at a finite value. This is likely due to the VOCs molecules accumulating themselves in a layer by layer fashion and inducing multiple-layer adsorptions at higher concentrations. The final frequency shift at saturated pressure (P/P_0 = 1.0) does not affect the affinity constants too much, since a single point will not decide the variation trend. To be consistent, we used the frequency shift after 10 min at P/P_0 = 1.0 as the response value at saturated concentration in practical usage of the sensor array.

DOI: 10.1021/acsami.5b04385
ACS Appl. Mater. Interfaces 2015, 7, 17893−17903

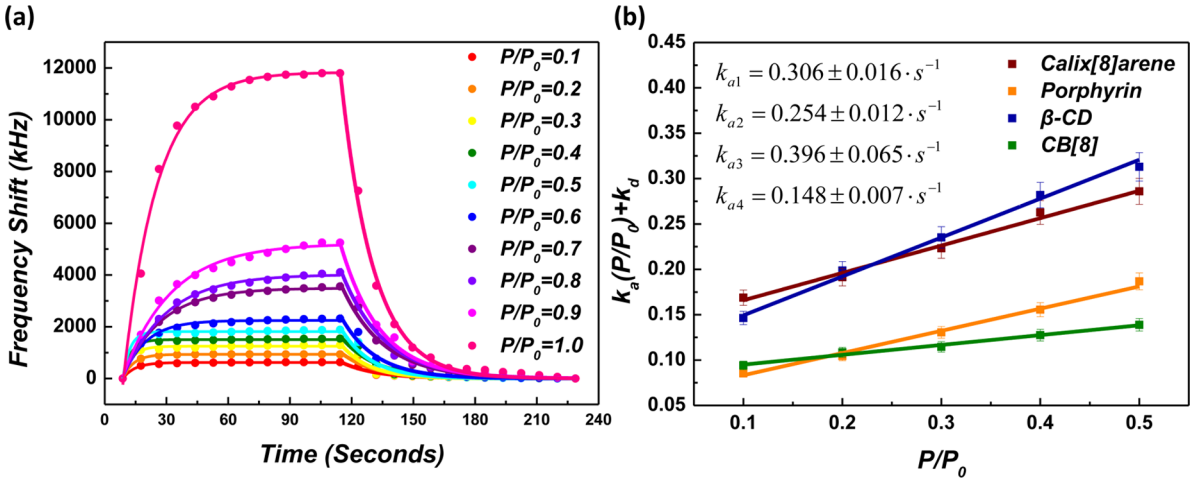

Figure 5. (a) Real-time sensor responses of chloroform adsorption and desorption processes on Calix[8]arene monolayer. The circles represent the measuring data, and the solid lines represent the fitting results. Here the minus values of frequency shifts were used to fit the monoexponential equations for convenience. (b) Plots of adsorption rates (k_a (P/P_0) + k_d) versus P/P_0 for chloroform adsorption. The linear fits of the data at P/P_0 = 0.1−0.5 give the adsorption rate constants k_{a1} = 0.306 ± 0.016 s^{-1}, k_{a2} = 0.254 ± 0.012 s^{-1}, k_{a3} = 0.396 ± 0.065 s^{-1}, k_{a4} = 0.148 ± 0.007 s^{-1}, respectively, for Calix[8]arene, Porphyrin, β-CD, and CB[8], monolayers.

Table 2. Adsorption and Desorption Rate Constants of Six VOCs Fitted by Monoexponential Equations

	adsorption/desorption							
	Calix[8]arene		Porphyrin		β-CD		CB[8]	
VOC	$k_a \times 10^{-1}$ (s^{-1})	$k_d \times 10^{-2}$ (s^{-1})	$k_a \times 10^{-1}$ (s^{-1})	$k_d \times 10^{-2}$ (s^{-1})	$k_a \times 10^{-1}$ (s^{-1})	$k_d \times 10^{-2}$ (s^{-1})	$k_a \times 10^{-1}$ (s^{-1})	$k_d \times 10^{-2}$ (s^{-1})
chloroform	3.06 ± 0.16	1.9 ± 0.5	2.54 ± 0.12	1.5 ± 0.4	3.96 ± 0.65	2.5 ± 0.7	1.48 ± 0.07	1.2 ± 0.6
acetone	4.58 ± 0.23	2.5 ± 0.4	1.34 ± 0.28	1.1 ± 0.6	4.78 ± 0.79	2.3 ± 0.7	2.37 ± 0.25	1.8 ± 0.5
NPA	2.42 ± 0.40	1.3 ± 0.7	1.92 ± 0.27	1.2 ± 0.6	3.23 ± 0.11	2.9 ± 0.4	0.99 ± 0.06	0.6 ± 0.7
methanol	2.08 ± 0.17	1.1 ± 0.4	1.55 ± 0.18	0.8 ± 0.8	5.69 ± 0.22	2.3 ± 0.5	1.05 ± 0.08	0.5 ± 0.4
hexane	4.74 ± 0.22	3.2 ± 0.3	0.82 ± 0.07	0.7 ± 0.7	4.47 ± 0.35	2.6 ± 0.6	1.89 ± 0.07	1.4 ± 0.4
cyclohexane	2.81 ± 0.07	2.8 ± 0.6	1.24 ± 0.11	1.3 ± 0.3	3.43 ± 0.31	2.7 ± 0.5	1.08 ± 0.10	1.6 ± 0.5

Dual-site Langmuir−Freundlich (DSLF) eq 2 was used to fit the adsorption isotherms, since the simple Langmuir model cannot match well with the experiment data.[46]

$$\Delta f = \frac{N_1 K_1 (P/P_0)^{n_1}}{1 + K_1 (P/P_0)^{n_1}} + \frac{N_2 K_2 (P/P_0)^{n_2}}{1 + K_2 (P/P_0)^{n_2}} \quad (2)$$

Here Δf is the frequency shift of a FBAR sensor which is linearly proportional to the total number of adsorbed gas molecules, N_i is the maximum loading in site i, K_i is the affinity constant, and n_i is used to characterize the deviation from the simple Langmuir equation (i = 1, 2). Adsorption isotherms of the other five VOCs (acetone, n-propyl alcohol (NPA), methanol, hexane, and cyclohexane) were fitted using the same DSLF equation (see Figure S5, Supporting Information). Two affinity constants K_1 and K_2 were obtained during the equation fitting and listed in Table 1.

According to the fitting results, the affinity constant K_1 shows larger distributions compared with K_2, which means two equivalent adsorption types simultaneously affect the adsorption isotherms and K_1 is more selective. This can be explained by the gas adsorption inside and outside of the supramolecular cavities (see Scheme 2). For affinity constant K_1, the gas molecules interact with the supramolecular functional groups and enter into the cavity of the supramolecules; thus, the value of K_1 is determined by both the sensing layers and the VOCs to be detected. The affinity constant K_2 can be used to describe the outside-cavity adsorption between two supramolecules on the substrate, and this interaction is determined only by the properties of VOCs.

3.4.3. Adsorption Kinetics of VOCs on Supramolecular Monolayers. Besides the adsorption isotherms, the kinetic analyses of different VOCs adsorption on four supramolecular monolayers were applied as well. The adsorption and desorption rates of different VOCs on the same sensitive coating are different, which is likely due to the polar or nonpolar characteristics of the VOCs molecules. And such distinction varies with supramolecular monolayers containing different functional groups on the gas−solid interface. Monoexponential eqs 3a and 3b were applied to fit the real-time adsorption and desorption data.[47−49]

$$\Delta f = f_{eq}\left(1 - e^{-(k_a(P/P_0)+k_d)t}\right) \quad (3a)$$

$$\Delta f = f_{eq}\, e^{-k_d t} \quad (3b)$$

Here f_{eq} is the frequency shift of FBAR sensor when VOCs adsorption reaches equilibrium and k_a and k_d are adsorption and desorption rate constant, respectively. The solid lines in Figure 5a represent the fitting results of chloroform adsorption on Calix[8]arene monolayer at 10 concentrations.

The desorption rate constants (k_d) were directly determined by fitting the desorption curves of different concentrations with eq 3b. The average values are k_{d1} = 0.019 ± 0.005 s^{-1}, k_{d2} = 0.015 ± 0.004 s^{-1}, k_{d3} = 0.025 ± 0.007 s^{-1}, k_{d4} = 0.012 ± 0.006 s^{-1}, respectively, for chloroform desorption from Calix[8]arene,

DOI: 10.1021/acsami.5b04385
ACS Appl. Mater. Interfaces 2015, 7, 17893−17903

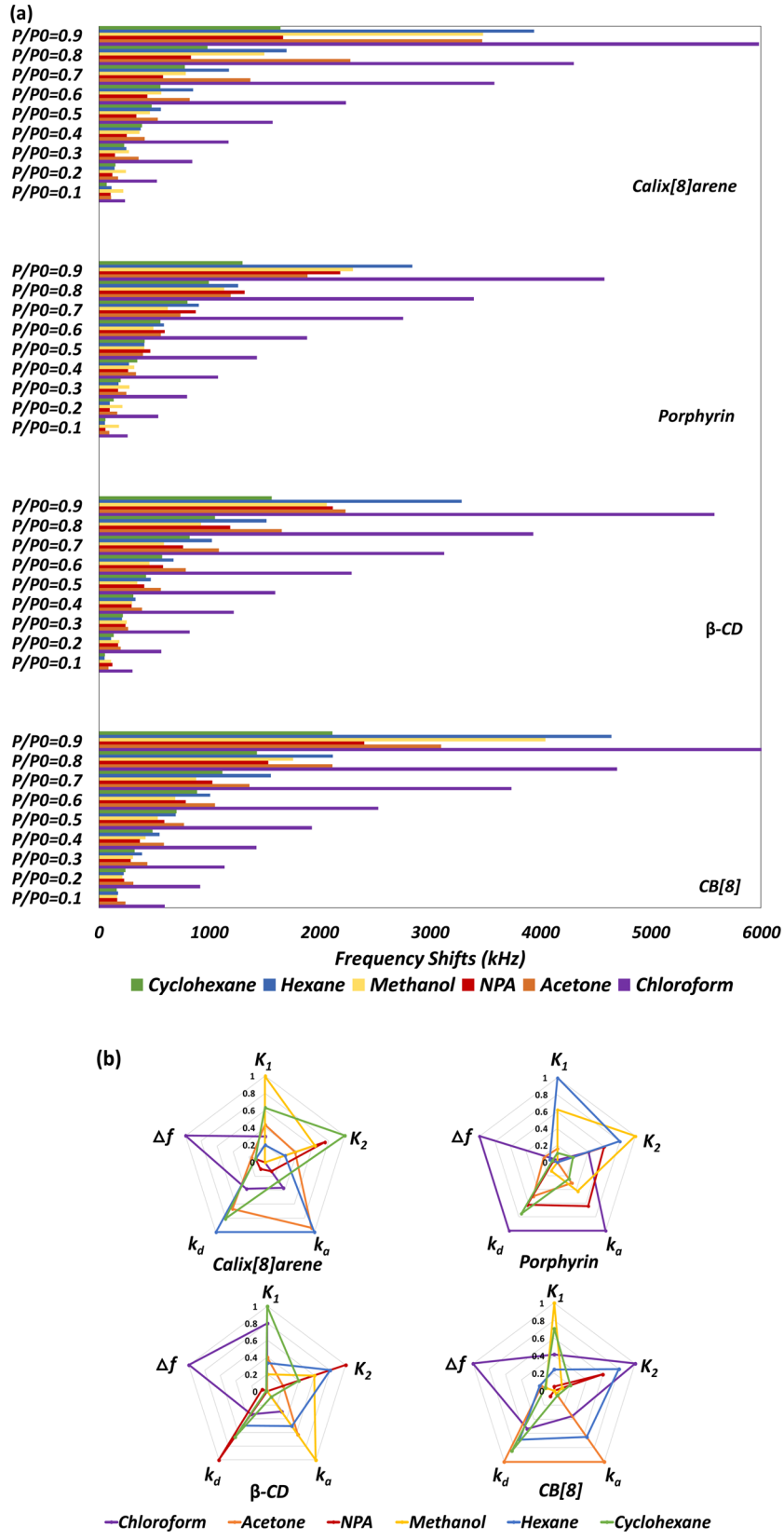

Figure 6. (a) Frequency responses of FBAR sensor array versus VOCs concentrations. (b) Radar plots of the sensor responses (normalized Δf, K_1, K_2, k_a, and k_d) for the fingerprint library of VOCs detection on Calix[8]arene, Porphyrin, β-CD, and CB[8].

Porphyrin, β-CD, and CB[8] monolayers. By fitting the adsorption curves (Figure 5a), the five obtained values of $(k_a(P/P_0) + k_d)$ were then plotted versus chloroform concentrations from $P/P_0 = 0.1-0.5$ (Figure 5b). The slopes of the fitted solid lines give the adsorption rate constants: $k_{a1} = 0.306 \pm 0.016\ s^{-1}$, $k_{a2} = 0.254 \pm 0.012\ s^{-1}$, $k_{a3} = 0.396 \pm 0.065$

DOI: 10.1021/acsami.5b04385
ACS Appl. Mater. Interfaces 2015, 7, 17893−17903

s^{-1}, k_{a4} = 0.148 ± 0.007 s^{-1}. It is likely that monolayer adsorption occurs at low concentration (P/P_0 below 0.5 for chloroform) which is suitable with simple Langmuir model, and the adsorption rates can be calculated using monoexponential eq 3a. In contrast, ($k_a(P/P_0) + k_d$) decreases after the turning point of P/P_0 = 0.5 and keeps almost the same value for P/P_0 = 0.6−1.0, which is likely due to the multiple layers gas adsorption with longer interaction time. The adsorption equilibrium constant k_d/k_a is close to the affinity constant (K_1) in the order of magnitudes. Differences are likely caused by the measuring deviations of the network analyzer. Adsorption and desorption rate constants of the other five VOCs are calculated using the same method; however, the turning points of VOCs concentrations P/P_0 between monolayer and multilayer gas adsorption vary with different VOCs (see Figure S6, Supporting Information). All the fitting results of adsorption and desorption rate constants are shown in Table 2.

Figure 6a shows the frequency shifts of the FBAR sensor array with exposure to different concentrations of six VOCs, which can be used as single-parameter fingerprints for the discrimination of VOCs. Along with the frequency shifts (Δf) from readable signals of the FBAR sensor array, parameters from adsorption isotherms (K_1, K_2) and kinetics analyses (k_a, k_d) inherent to the supramolecular "host−guest" interactions constitute a distinctive matrix (Δf, K_1, K_2, k_a, k_d) of different VOCs, which can be used as a multiparameter recognition fingerprint for the classification of VOCs. Figure 6b shows the radar plots of the sensor responses containing five normalized parameters (Δf, K_1, K_2, k_a, k_d). Different VOCs display distinctive patterns with the functionalized FBAR sensor array, thus allowing for a simple and straightforward identification of the VOCs to be detected.

The frequency shifts of the functionalized FBAR sensor array (Figure 6a) display a concentration-dependent behavior when exposed to different concentrations of VOCs and can be used in the concentration detection, while the additional sensing parameters (K_1, K_2, k_a, k_d) of each VOC is kept constant regardless the concentration (see Figure 6b) and can be used for the classification of VOCs.

So far we have demonstrated an e-nose type gas sensor that is composed of microfabricated resonators functionalized individually with different supramolecular monolayers to enhance the sensitivity toward different VOCs. However, regarding the real samples, a preconcentrator is normally integrated before the gas sensor array to separate the gas mixtures and to concentrate the VOCs which will further improve the limit of detection (LOD) of the e-noses.[50]

4. CONCLUSIONS

In this work, a FBAR sensor array functionalized with four supramolecular monolayers (Calix[8]arene, Porphyrin, β-CD, and CB[8]) has been demonstrated for selective detection of VOCs through frequency shifts and analyses of adsorption isotherms/kinetics through the specific "host−guest" gas phase recognitions. To our knowledge, these results are the first experimental demonstration that the microfabricated resonator array can be used as high-throughput sensors to quantify gas molecule−supramolecular monolayer interactions. The supramolecular monolayers were fabricated on FBAR surfaces using LB techniques. Compression isotherms, contact angle (CA) measurements, Fourier transform infrared (FT-IR) spectrometry, and atomic force microscopy (AFM) were used to verify the formation of the supramolecular monolayers. The ultrahigh frequency FBAR transducers working at 4.4 GHz enhanced their sensitivity to gas molecules, thus enabling the detection of VOCs with the monolayer coatings. Fitting with a dual-site Langmuir−Freundlich equation, two affinity constants (K_1, K_2) were obtained that are representing inside- and outside-supramolecular cavity adsorption. Furthermore, kinetics analyses derived the adsorption and desorption rate constants (k_a, k_d) of VOCs on different supramolecular monolayers. All the parameters from adsorption isotherms and kinetic analyses along with frequency shifts constituted a matrix (Δf, K_1, K_2, k_a, k_d) as parts of the fingerprint library for VOCs selective detections and discriminations. Compared with the conventional single parameter sensing (e.g., only with frequency shifts from acoustic wave transducers), the multiple parameter sensing by supramolecular monolayers functionalized FBAR sensor array can detect VOCs with high specificity and selectivity, which is a promising candidate for the development of e-nose systems.

■ ASSOCIATED CONTENT

Supporting Information

The Supporting Information is available free of charge on the ACS Publications website at DOI: 10.1021/acsami.5b04385.

FBAR microfabrication process, VOCs detection setup, Contact angle images, Real-time sensor responses of the FBAR sensor array, Adsorption isotherms and kinetics of VOCs on supramolecular monolayers (PDF)

■ AUTHOR INFORMATION

Corresponding Authors

*W.P.: e-mail, weipang@tju.edu.cn.

*X.D.: e-mail, xduan@tju.edu.cn; tel/fax, +86 2227401002.

Notes

The authors declare no competing financial interest.

■ ACKNOWLEDGMENTS

The authors gratefully acknowledge financial support in part from the Natural Science Foundation of China (NSFC No. 61176106) and the 111 Project (Grant B07014). X.D. acknowledges support by the Tianjin Applied Basic Research and Advanced Technology (Grant 14JCYBJC41500).

■ REFERENCES

(1) Paska, Y.; Stelzner, T.; Assad, O.; Tisch, U.; Christiansen, S.; Haick, H. Molecular Gating of Silicon Nanowire Field-Effect Transistors with Nonpolar Analytes. *ACS Nano* **2012**, *6*, 335−345.

(2) Konvalina, G.; Haick, H. Sensors for Breath Testing: From Nanomaterials to Comprehensive Disease Detection. *Acc. Chem. Res.* **2014**, *47*, 66−76.

(3) Wang, B.; Haick, H. Effect of Chain Length on the Sensing of Volatile Organic Compounds by Means of Silicon Nanowires. *ACS Appl. Mater. Interfaces* **2013**, *5*, 5748−5756.

(4) Lichtenstein, A.; Havivi, E.; Shacham, R.; Hahamy, E.; Leibovich, R.; Pevzner, A.; Krivitsky, V.; Davivi, G.; Presman, I.; Elnathan, R.; Engel, Y.; Flaxer, E.; Patolsky, F. Supersensitive Fingerprinting of Explosives by Chemically Modified Nanosensors Arrays. *Nat. Commun.* **2014**, *5*, 4195−4206.

(5) Hakim, M.; Broza, Y. Y.; Barash, O.; Peled, N.; Phillips, M.; Amann, A.; Haick, H. Volatile Organic Compounds of Lung Cancer and Possible Biochemical Pathways. *Chem. Rev.* **2012**, *112*, 5949−5966.

DOI: 10.1021/acsami.5b04385
ACS Appl. Mater. Interfaces 2015, 7, 17893−17903

(6) Tisch, U.; Billan, S.; Ilouze, M.; Phillips, M.; Peled, N.; Haick, H. Volatile Organic Compounds in Exhaled Breath as Biomarkers for the Early Detection and Screening of Lung Cancer. *Lung Cancer* **2012**, *5*, 107−117.
(7) Adiguzel, Y.; Kulah, H. Breath Sensors for Lung Cancer Diagnosis. *Biosens. Bioelectron.* **2015**, *65*, 121−138.
(8) Shehada, N.; Bronstrup, G.; Funka, K.; Christiansen, S.; Leja, M.; Haick, H. Ultrasensitive Silicon Nanowire for Real-world Gas Sensing: Noninvasive Diagnosis of Cancer from Breath Volatolome. *Nano Lett.* **2015**, *15*, 1288−1295.
(9) Suslick, B. A.; Feng, L.; Suslick, K. S. Discrimination of Complex Mixtures by a Colorimetric Sensor Array: Coffee Aromas. *Anal. Chem.* **2010**, *82*, 2067−2073.
(10) Rock, F.; Barsan, N.; Weimar, U. Electronic Nose: Current Status and Future Trends. *Chem. Rev.* **2008**, *108*, 705−725.
(11) Di Natale, C.; Paolesse, R.; Macagnano, A.; Mantini, A.; D'Amico, A.; Legin, A.; Lvova, L.; Rudnitskaya, A.; Vlasov, Y. Electronic Nose and Electronic Tongue Integration for Improved Classification of Clinical and Food Samples. *Sens. Actuators, B* **2000**, *64*, 15−21.
(12) Kimura, M.; Sakai, R.; Sato, S.; Fukawa, T.; Ikehara, T.; Maeda, R.; Mihara, T. Sensing of Vaporous Organic Compounds by TiO_2 Porous Films Covered with Polythiophene Layers. *Adv. Funct. Mater.* **2012**, *22*, 469−476.
(13) Ko, W.; Jung, N.; Lee, M.; Yun, M.; Jeon, S. Electronic Nose Based on Multipatterns of ZnO Nanorods on a Quartz Resonator with Remote Electrodes. *ACS Nano* **2013**, *7*, 6685−6690.
(14) Yang, W.; Wan, P.; Jia, M.; Hu, J.; Guan, Y.; Feng, L. A Novel Electronic Nose Based on Porous In_2O_3 Microtubes Sensor Array for the Discrimination of VOCs. *Biosens. Bioelectron.* **2015**, *64*, 547−553.
(15) Ferrari, V.; Marioli, D.; Taroni, A.; Ranucci, E. Multisensor Array of Mass Microbalances for Chemical Detection Based on Resonant Piezo-layers of Screen-printed PZT. *Sens. Actuators, B* **2000**, *68*, 81−87.
(16) Li, D.; Ma, M. Surface Acoustic Wave Microsensors Based on Cyclodextrin Coatings. *Sens. Actuators, B* **2000**, *69* (1), 75−84.
(17) Lu, C. J.; Whiting, J.; Sacks, R. D.; Zellers, E. T. Portable Gas Chromatograph with Tunable Retention and Sensor Array Detection for Determination of Complex Vapor Mixtures. *Anal. Chem.* **2003**, *75*, 1400−1409.
(18) Alizadeh, T.; Zeynali, S. Electronic Nose Based on the Polymer Coated SAW Sensors Array for the Warfare Agent Simulants Classification. *Sens. Actuators, B* **2008**, *129*, 412−423.
(19) Pang, W.; Zhao, H.; Kim, E. S.; Zhang, H.; Yu, H.; Hu, X. Piezoelectric Microelectromechanical Resonant Sensors for Chemical and Biological Detection. *Lab Chip* **2012**, *12*, 29−44.
(20) Okahata, Y.; Matsuura, K.; Ito, K.; Ebara, Y. Gas-phase Selective Adsorption on Functional Monolayers Immobilized on a Highly Sensitive Quartz-crystal Microbalance. *Langmuir* **1996**, *12*, 1023−1026.
(21) Yamagiwa, H.; Sato, S.; Fukawa, T.; Ikehara, T.; Maeda, R.; Mihara, T.; Kimura, M. Detection of Volatile Organic Compounds by Weight-detectable Sensors Coated with Metal-organic Frameworks. *Sci. Rep.* **2014**, *4*, 6247−6252.
(22) Arshak, K.; Moore, E.; Lyons, G. M.; Harris, J.; Clifford, S. A Review of Gas Sensors Employed in Electronic Nose Applications. *Sens. Rev.* **2004**, *24*, 181−198.
(23) Erdogan, M.; Özbek, Z.; Çapan, R.; Yagci, Y. Characterization of Polymeric LB Thin Films for Sensor Applications. *J. Appl. Polym. Sci.* **2012**, *123*, 2414−2422.
(24) Lee, C. Y.; Strano, M. S. Understanding the Dynamics of Signal Transduction for Adsorption of Gases and Vapors on Carbon Nanotube Sensors. *Langmuir* **2005**, *21*, 5192−5196.
(25) Zhang, T.; Mubeen, S.; Myung, N. V.; Deshusses, M. A. Recent Progress in Carbon Nanotube-based Gas Sensors. *Nanotechnology* **2008**, *19*, 332001−332014.
(26) Pirondini, L.; Dalcanale, E. Molecular Recognition at the Gas-solid Interface: A Powerful Tool for Chemical Sensing. *Chem. Soc. Rev.* **2007**, *36*, 695−706.
(27) Sun, P.; Jiang, Y.; Xie, G.; Du, X.; Hu, J. A Room Temperature Supramolecular-based Quartz Crystal Microbalance (QCM) Methane Gas sensor. *Sens. Actuators, B* **2009**, *141*, 104−108.
(28) Brutschy, M.; Lubczyk, D.; Mullen, K.; Waldvogel, S. R. Surface Pretreatment Boosts the Performance of Supramolecular Affinity Materials on Quartz Crystal Microbalances for Sensor Applications. *Anal. Chem.* **2013**, *85*, 10526−30.
(29) Mattia, E.; Otto, S. Supramolecular Systems Chemistry. *Nat. Nanotechnol.* **2015**, *10*, 111−119.
(30) Capan, İ.; Tarımcı, Ç.; Capan, R. Fabrication of Langmuir−Blodgett Thin Films of Porphyrins and Investigation on Their Gas Sensing Properties. *Sens. Actuators, B* **2010**, *144*, 126−130.
(31) Çaycı, D.; Stanciu, S. G.; Çapan, İ.; Erdoğan, M.; Güner, B.; Hristu, R.; Stanciu, G. A. The Influence of the Surface Morphologies of Langmuir Blodgett (LB) Thin Films of Porphyrins on their gas sensing properties. *Sens. Actuators, B* **2011**, *158*, 62−68.
(32) Capan, İ.; Erdoğan, M.; Stanciu, G. A.; Stanciu, S. G.; Hristu, R.; Göktepe, M. The Interaction between the Gas Sensing and Surface morphology Properties of LB Thin Films of Porphyrins in Terms of the Adsorption Kinetics. *Mater. Chem. Phys.* **2012**, *136*, 1130−1136.
(33) Çapan, R.; Özbek, Z.; Göktaş, H.; Şen, S.; İnce, F. G.; Özel, M. E.; Stanciu, G. A.; Davis, F. Characterization of Langmuir−Blodgett Films of a Calix[8]arene and Sensing Properties towards Volatile Organic Vapors. *Sens. Actuators, B* **2010**, *148*, 358−365.
(34) Ozmen, M.; Ozbek, Z.; Bayrakci, M.; Ertul, S.; Ersoz, M.; Capan, R. Preparation and Gas Sensing Properties of Langmuir−Blodgett Thin Films of Calix[n]arenes: Investigation of Cavity Effect. *Sens. Actuators, B* **2014**, *195*, 156−164.
(35) Ozmen, M.; Ozbek, Z.; Buyukcelebi, S.; Bayrakci, M.; Ertul, S.; Ersoz, M.; Capan, R. Fabrication of Langmuir−Blodgett Thin Films of Calix[4]arenes and Their Gas Sensing Properties: Investigation of Upper Rim Para Substituent Fffect. *Sens. Actuators, B* **2014**, *190*, 502−511.
(36) Zhang, H.; Marma, M. S.; Bahl, S. K.; Kim, E. S.; McKenna, C. E. Sequence Specific Label-Free DNA Sensing Using Film-Bulk-Acoustic-Resonators. *IEEE Sens. J.* **2007**, *7*, 1587−1588.
(37) Zhang, M.; Huang, J.; Cui, W.; Pang, W.; Zhang, H.; Zhang, D.; Duan, X. Kinetic Studies of Microfabricated Biosensors Using Local Adsorption Strategy. *Biosens. Bioelectron.* **2015**, *74*, 8−15.
(38) Chen, D.; Xu, Y.; Wang, J.; Zhang, L. Nerve Gas Sensor Using Film Bulk Acoustic Resonator Modified with a Self-assembled Cu^{2+}/11-mercaptoundecanoic Acid Bilayer. *Sens. Actuators, B* **2010**, *150*, 483−486.
(39) Hashimoto, K. Y. *RF Bulk Acoustic Wave Filters for Communications*, 1st ed; Artech House: London, 2009.
(40) Liu, W.; Wang, J.; Yu, Y.; Chang, Y.; Tang, N.; Qu, H.; Wang, Y.; Pang, W.; Zhang, H.; Zhang, D. Tuning the Resonant Frequency of Resonators Using Molecular Surface Self-assembly Approach. *ACS Appl. Mater. Interfaces* **2015**, *7*, 950−958.
(41) Li, L.-S.; Da, S.-L.; Feng, Y.-Q.; LIU, M. Preparation and Characterization of a New p-tert-butyl-calix[8]arene-bonded Stationary Phase for High-performance Liquid Chromatography. *Anal. Sci.* **2004**, *20*, 561−564.
(42) Thomas, D. W.; Martell, A. E. Absorption Spectra of Para-Substituted Tetraphenyl Porphines 1, 2. *J. Am. Chem. Soc.* **1956**, *78*, 1338−1343.
(43) Teixeira, L. R.; Sinisterra, R. D.; Vieira, R. P.; Doretto, M. C.; Beraldo, H. Inclusion of Benzaldehyde Semicarbazone into *β*-Cyclodextrin Produces a Very Effective Anticonvulsant Formulation. *J. Inclusion Phenom. Mol. Recognit. Chem.* **2003**, *47*, 77−82.
(44) Hu, H.; Xin, J. H.; Hu, H.; Wang, X.; Lu, X. Organic Liquids-responsive Beta-cyclodextrin-functionalized Graphene-based Gluorescence Probe: Label-free Selective Detection of Tetrahydrofuran. *Molecules* **2014**, *19*, 7459−7479.
(45) Victor, S. P.; Paul, W.; Jayabalan, M.; Sharma, C. P. Cucurbituril/hydroxyapatite Based Nanoparticles for Potential Use in Theranostic Applications. *CrystEngComm* **2014**, *16*, 6929−6936.
(46) Babarao, R.; Hu, Z.; Jiang, J.; Chempath, S.; Sandler, S. I. Storage and Separation of CO_2 and CH_4 in Silicalite, C_{168} Schwarzite,

DOI: 10.1021/acsami.5b04385
ACS Appl. Mater. Interfaces 2015, 7, 17893−17903

and IRMOF-1: A Comparative Study from Monte Carlo Simulation. *Langmuir* **2007**, *23*, 659−666.
(47) Duan, X.; Li, Y.; Rajan, N. K.; Routenberg, D. A.; Modis, Y.; Reed, M. A. Quantification of the Affinities and Kinetics of Protein Interactions Using Silicon Nanowire Biosensors. *Nat. Nanotechnol.* **2012**, *7*, 401−407.
(48) Kondo, A.; Kojima, N.; Kajiro, H.; Noguchi, H.; Hattori, Y.; Okino, F.; Maeda, K.; Ohba, T.; Kaneko, K.; Kanoh, H. Gas Adsorption Mechanism and Kinetics of an Elastic Layer-Structured Metal−Organic Framework. *J. Phys. Chem. C* **2012**, *116*, 4157−4162.
(49) Al-Marri, M. J.; Khader, M. M.; Tawfik, M.; Qi, G.; Giannelis, E. P. CO_2 Sorption Kinetics of Scaled-Up Polyethylenimine-Functionalized Mesoporous Silica Sorbent. *Langmuir* **2015**, *31*, 3569−3576.
(50) Lahlou, H.; Vilanova, X.; Correig, X. Gas Phase Micropreconcentrators for Benzene Monitoring: A Review. *Sens. Actuators, B* **2013**, *176*, 198−210.

DOI: 10.1021/acsami.5b04385
ACS Appl. Mater. Interfaces 2015, 7, 17893−17903